59 SYNOPTIC INFLUENCE ON HIGH SHEAR LOW CAPE EVENTS

Jessica R. King* and Matthew D. Parker
North Carolina State University, Raleigh, North Carolina

1. INTRODUCTION

High shear, low CAPE (HSLC) environments are common in the Southeastern, Mid-Atlantic, Tennessee Valley and Ohio Valley regions of the United States (Guyer et al. 2006; Smith et al. 2008). Recent studies regarding severe weather climatology and false alarm rates (e.g., Guyer and Dean 2010; Brotzge et al. 2011; Coleman and Dixon 2013) have recognized HSLC convective events as a significant threat to the regions in which they occur.

HSLC severe events are typically small in horizontal scale and are low-topped, which can lead to a low probability of detection by radar (Brotzge et al. 2011). In addition, HSLC events commonly occur during the cool season (Sherburn and Parker 2014) and overnight (Guyer and Dean 2010), imposing an even larger threat to communities may not be aware of the convective risk. Recent efforts to improve the forecasts of HSLC events and reduce false alarm rates have included focusing on tornadic radar signatures (e.g., Clark 2011; Davis and Parker 2014), while other studies have concentrated more on the environmental conditions in which HSLC storms develop (e.g., Clark 2014; Sherburn and Parker 2014).

Previous studies have suggested the possible importance of a dry intrusion in the middle levels and the release of potential instability in HSLC events (Lane and Moore 2006; Clark 2009). Similarly, several studies throughout the past decade have deduced that HSLC severe events are strongly synoptically forced events (e.g., Wheatley and Trapp 2008; Clark 2009; Dial et al. 2010), unlike higher CAPE convection that typically occurs during the warm season, and may be linked to weaker mesoscale heterogeneity. Jewett and Wilhelmson (2006) found synoptic frontal circulations to have a significant influence on the storm morphology of cool season mesoscale convective systems (MCSs). Coniglio et al. (2007) found similar results, although they noted that surging outflow from the system may have an additional influence on storm maintenance. This ongoing study examines the relationship of the synoptic environment to the development of HSLC convective systems.

* *Corresponding author address*: Jessica R. King, Department of Marine, Earth and Atmospheric Sciences, North Carolina State University, Raleigh, NC 27607; e-mail: jrking2@ncsu.edu.

2. METHODS

Real-data simulations of two separate HSLC events have been performed. Both of the events took place during the cool season in the Tennessee/Ohio Valley, and appeared to be somewhat synoptically forced. An idealized simulation absent of synoptic effects was also performed for comparison.

Two real-data numerical simulations were performed using the fully compressible, non-hydrostatic Advanced Research Weather Research and Forecasting model (WRF-ARW; Skamarock 2008), version 3.5.1. The two events simulated include a quasi-linear convective system (QLCS) that occurred on January 30 of 2013, and a QLCS with leading individual cells that occurred on February 5, 2008. These events were both high impact events, producing several tornadoes in addition to intense surface winds (see Figs. 3b and 8b for severe reports). Each simulation was run for 30 hours to account for the evolution of both the synoptic and the mesoscale environments. An outer domain at 9 km grid spacing was one-way nested down to an inner domain at 3 km grid spacing (Fig. 1). The vertical grid had 50 pressure levels. Initial conditions were supplied by the NAM 12 km analysis and boundary conditions were updated on 6 hour intervals. Cumulus convection was parameterized on the outer domain by Kain-Fritsch scheme (Kain 2004). Other important parameterization methods include the WSM-6 class graupel microphysical scheme (Hong et al. 2006) and the Yonsei University (YSU) planetary boundary layer scheme (Noh et al. 2003). The simulations reasonably replicated the reflectivity structure and accumulated precipitation of the observed convective events.

An idealized numerical simulation was performed using Bryan's cloud model (CM1: Bryan and Fritsch 2002), version 17. The simulation was completed on a 400 km x 100 km grid with 1 km grid spacing. The vertical grid had 48 model levels. A cold wedge of -8 K was initialized having a maximum height of 4 km and a width of 100 km. Random perturbations of 0.20 K were also included to permit 3D structures to

emerge. The Morrison double-moment scheme (Morrison et al. 2005) was used for precipitation microphysics. The base-state thermodynamic and wind profile initialized in the idealized simulation correspond with those of the pre-convective environment in the first real-data simulation. The idealized simulation was run for 420 minutes (7 hours). Coriolis acceleration was not included in this simulation.

3. AN OVERVIEW OF THE REAL-DATA SIMULATIONS

3.1 January 30, 2013

On January 29, 2013, a deep upper trough centered over the western plains began to lift as it progressed eastward. A QLCS began to form along the associated surface cold front around 13 UTC in the plains. The QLCS extended southwest from eastern Wisconsin into north-central Texas by 00 UTC on January 30, just downstream of the upper trough (Fig. 2; Fig. 3a,c). By 06 UTC on January 30, the QLCS had intensified and began to push through the Ohio, Tennessee and Mississippi Valleys, inducing significant winds and several tornados along the leading line (See Fig. 3b for reports). The following discussion will refer to the simulation of this event.

As the simulated QLCS moves eastward into the late evening, simulated surface CAPE depletes rather quickly. Areas in northern Tennessee and Kentucky have less than 400 J kg^{-1} of CAPE as the convective line approaches (Fig. 4). The environment is relatively dry and stable at 03 UTC, approximately 6 hours before the line passes (Fig. 5a). Low-level shear is on the order of 50 kts with storm relative effective helicity (SREH) values over 400 $m^2 s^{-2}$.

The QLCS propagates along an outflow boundary, originating from upstream, higher CAPE convection, and surges eastward ahead of the surface cold front (Fig. 6). Intense low-level flow from the southwest (Fig. 12a) supplies immense amounts of moisture to the dry low-levels of the pre-convective environment in addition to increasing vertical wind shear as the outflow boundary approaches. The environment destabilizes rapidly as moistening occurs, producing sufficient increases in CAPE by the time of arrival of the outflow boundary (see soundings in Fig. 5). Once the line passes, surface θ_e values drop over 15 K, and the environment is rapidly stabilized by the cold air behind the leading outflow line.

The pre-convective environment in this case evolves over a relatively short time period of a few hours. Strong, southwesterly low-level flow moistens the low levels, and the environment is destabilized. The HSLC convection in this case occurs along outflow that emanates from higher CAPE convection that originated in Texas and Oklahoma earlier in the day.

3.2 *February 5, 2008*

On the afternoon of February 5, 2008, convection began to develop in eastern Texas and Oklahoma, downstream of a deep upper level trough in the warm sector of an associated surface cyclone (Figs. 7, 8a). By 18 UTC on February 5, unorganized convection had developed downstream of the deepening upper trough in the warm sector of the enhanced surface cyclone (Fig. 8c). A QLCS began to form as convection became more organized approaching the Ohio Valley. The QLCS in addition to more isolated cells out ahead produced several intense tornadoes and severe winds (Fig. 8b). The following discussion will refer to the simulation of this event.

Simulated CAPE, although larger farther to the south, is still well below 500 J kg^{-1} (Fig. 9) as the isolated cells approach the Ohio Valley. The mid-levels of the environment are relatively dry at 23 UTC, just a few hours before convection occurs (Fig. 10a). Extreme vertical shear is present throughout the low levels, and SREH values reach over 500 $m^2 s^{-2}$.

The pre-convective environment rapidly moistens and destabilizes over the few hours prior to the arrival of convection (Fig. 10). Much like in the previous case, intense low-level flow increases low-level shear in addition to providing immense amounts of moisture to the low and mid-levels of the pre-convective environment (Fig. 12b). Outflow also appears to correspond with the intense convection occurring in southwestern Kentucky in this case; however, the outflow from upstream convection in this particular simulation forms more pocket-like structures (Fig. 11) instead of a surging line as in the previously discussed simulation.

Overall, the pre-convective environment in this case also changes quickly as strong low-level flow moistens and destabilizes the environmental profile. HSLC convection occurs along somewhat isolated pockets of convective outflow that appears to originate from higher CAPE convection occurring in the southern plains earlier in the day.

4. A BRIEF DISCUSSION OF THE IDEALIZED SIMULATION

The idealized simulation was initialized with the sounding in Fig. 6a, which corresponds with the thermodynamic and wind profile at 06 UTC on January 30, 2013 approximately 4 hours prior to the arrival of the convective line.

Reflectivity (not shown) confirms that weak, disorganized convection did occur in this simulation. However, when comparing the evolution the local profile of θ_e and water vapor mixing ratio (q_v) between the idealized simulation and the corresponding real-data simulation (Fig. 13), it is evident that the environment is not modified to the same extent over time in the idealized simulation as in the real-data simulation. Other parameters (e.g., vertical motion; not shown) indicate that the convection in the idealized model was much weaker and less organized the real-data simulated convection which included the full synoptic evolution.

5. IMPLICATIONS AND CONCLUSIONS

The far field soundings in both of the real-data simulations indicate dry intrusions in the mid-levels. Over a relatively short time period (approximately 4 hours), the dry layer in the pre-convective environment moistens almost entirely as convection approaches. A general increase in surface CAPE and θ_e can be seen in Fig. 14, peaking at the time that maximum vertical velocity also peaks. This suggests that the potential instability release mechanism may indeed be of importance in these cases. However, it appears that the increases in CAPE are primarily a result of the moistening of the mid-levels owing to the strong, moist low-level flow (Fig. 12).

The lifting mechanism in both of these cases also appears to be related to an outflow boundary that may emanate from higher CAPE convection. A surging outflow line from upstream convection in the first analyzed case corresponds with the intense HSLC convective line. In the second case, pockets of outflow from upstream cells influence convection in the HSLC environment. Thus, in both cases, it appears that the upstream convection has an influence on the HSLC convection that occurs. Other than its significance in generating outflow boundaries, upstream convection may also have a role in modifying the low-level flow and moisture fields ahead of HSLC storms by the diabatic generation of potential vorticity (Mahoney and Lackmann 2007), or possibly by other mechanisms.

In the real-data simulations, it appears that the synoptic environment plays a significant role in the evolution of the HSLC convective environment, especially in providing intense low and mid-level flow from the south and southwest. In the idealized simulation, the intense moistening and destabilization does not occur in the absence of synoptic effects, and convection to the degree of that in the real-data simulations does not occur.

6. FUTURE WORK

Upstream convection, which may be higher CAPE convection, appears to be of importance in the cases simulated in this study. We intend to clarify the roles of the upstream convection and the mechanisms by which upstream convection may condition the environment for HSLC storms that occur. In addition, we seek to quantify the moistening and destabilization that occurs in the pre-convective environment through thermodynamic budgets. In the two cases presented in this study, the environment evolves on the order of a few hours which can present extreme difficulty for operational forecasting purposes. We propose examining additional HSLC cases to determine if this rapid evolution is common to other events. We also intend to examine HSLC cases that appear to less synoptically forced as well as null HSLC events.

ACKNOWLEDGEMENTS

We acknowledge that this research would not have been possible without funding from NSF grant AGS-1156123 and NOAA grant NA14NWS4680013. We would like to thank Gary Lackmann for his input during the initial steps of this project, as well as the members of the N.C. State Convective Storms Group for their continued help and support. We would also like to thank our collaborators from the National Weather Service for their input and feedback throughout this ongoing research.

REFERENCES

Brotzge, J., S. Erickson, and H. Brooks, 2011: A 5-yr Climatology of Tornado False Alarms. *Wea. Forecasting*, **26**, 534-544.

Bryan, G. H., and J. M. Fritsch, 2002: A benchmark simulation for moist nonhydrostatic numerical models. *Mon. Wea. Rev*., **130**, 2917-2928.

Coleman, T. A., and P. Grady Dixon, 2014: An Objective Analysis of Tornado Risk in the United States. *Wea. Forecasting*, **29**, 366–376.

Clark, M. R., 2009: The southern England tornadoes of 30 December 2006: Case study of a tornadic storm in a low CAPE, high shear environment. *J. Atmos. Res.*, **93**, 50-65.

Clark, M. R., 2011: Doppler radar observations of mesovortices within a cool-season tornadic squall line over the UK. *J. Atmos. Res.*, **100**, 749-764.

Clark, M. R., and D. J. Parker, 2014: On the Mesoscale Structure of Surface Wind and Pressure Fields near Tornadic and Nontornadic Cold Fronts. *Mon. Wea. Rev.*, **142**, 3560–3585.

Coniglio, M. C., H. E. Brooks, S. J. Weiss, and S. F. Corfidi, 2007: Forecasting the Maintenance of Quasi-Linear Mesoscale Convective Systems. *Wea. Forecasting*, **22**, 556–570.

Davis, J. M., and M. D. Parker, 2014: Radar Climatology of Tornadic and Nontornadic Vortices in High-Shear, Low-CAPE Environments in the Mid-Atlantic and Southeastern United States. *Wea. Forecasting*, **29**, 828–853.

Dial, G. L., J. P. Racy, and R. L. Thompson, 2010: Short-term convective mode evolution along synoptic boundaries. *Wea. Forecasting*, **25**, 1430-1446.

Guyer, J.L., D.A. Imy, A. Kis, and K. Venable, 2006: Cool season significant (F2-F5) tornadoes in the Gulf Coast States. Preprints, *23nd Conf. Severe Local Storms*, St. Louis MO.

Hong, S., and J. J. Lim, 2006: The WRF single-moment 6-class microphysics scheme (WSM6). *J. Kor. Meteor. Soc.*, **42,** 129–151.

Jewett, B.F., and R.B. WIlhelmson 2006: The role of forcing in cell morphology and evolution within midlatitude squall lines. *Mon. Wea. Rev.,* **134**, 3714-3734.

Kain, J. S., 2004: The Kain–Fritsch convective parameterization: An update. *J. Appl. Meteor*., **43**, 170–181.

Lane, J. D., and P. D. Moore, 2006: Observations of a non-supercell tornadic thunderstorm from terminal Doppler weather radar. Preprints, *23rd Conf. on Severe Local Storms*, St. Louis, MO, Amer. Meteor. Soc., P4.5.

Mahoney, K. M., and G. M. Lackmann, 2007: The Effect of Upstream Convection on Downstream Precipitation. *Wea. Forecasting*, **22**, 255–277.

Morrison, H., J. A. Curry, and V. I. Khvorostyanov, 2005: A new double-moment microphysics parameterization for application in cloud and climate models. Part I: Description. *J. Atmos. Sci*., **62**, 1665-1677.

Noh, Y., W. G. Cheon, S.-Y. Hong, and S. Raasch, 2003: Improvement of the K-profile model for the planetary boundary layer based on large eddy simulation data. *Bound.-Layer Meteor*.,**107**, 401–427.

Sherburn, K. D., and M. D. Parker, 2014: Climatology and Ingredients of Significant Severe Convection in High-Shear, Low-CAPE Environments. *Wea. Forecasting*, **29**, 854–877.

Skamarock, W., J.B. Klemp, J. Dudhia (more) , 2008: A Description of the Advanced Research WRF Version 3. NCAR Technical Note NCAR/TN-475+STR

Smith, B.T., J.L. Guyer and A.R. Dean, 2008: The climatology, convective mode, and mesoscale environment of cool season severe thunderstorms in the Ohio and Tennessee Valleys, 1995-2006. Preprints, *24th Conf. Severe Local Storms*, Savannah GA.

Wheatley, D.M., and R. J. Trapp, 2008: The effect of mesoscale heterogeneity on the genesis and structure of mesovortices within quasi-linear convective systems. *Mon. Wea. Rev.*, **136**, 4220–4241.

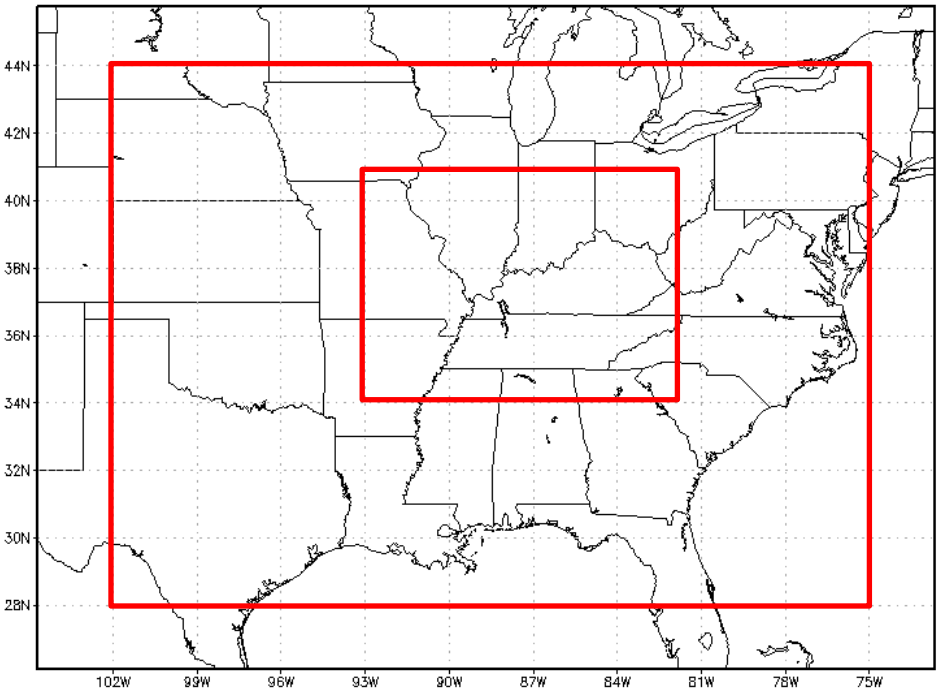

Fig. 1: Domains 1 (outer box, 9 km grid spacing) and 2 (inner box, 3 km grid spacing) for WRF-ARW real-data simulations.

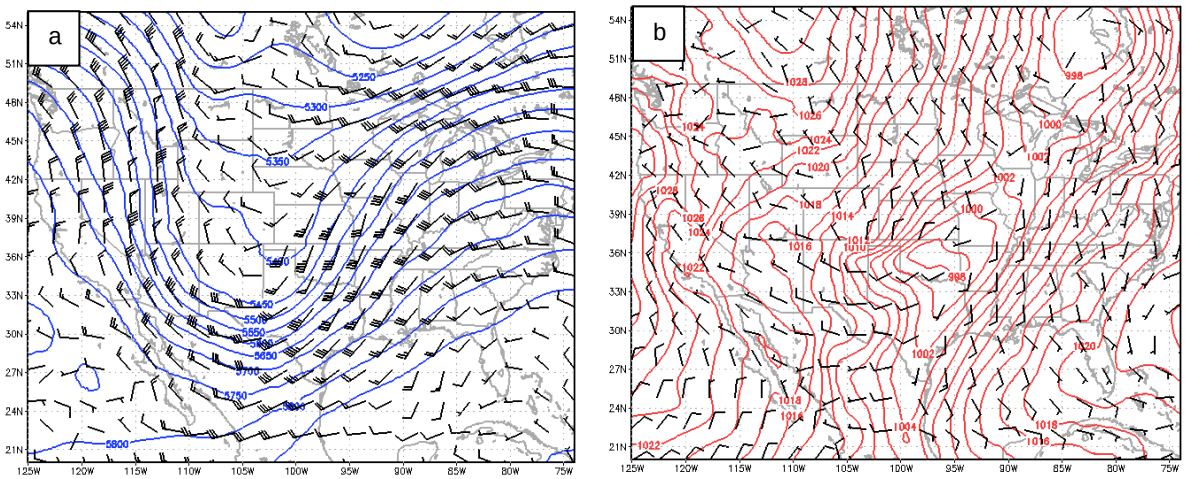

Fig. 2: (a) 500mb heights [m] and winds [m s^{-1}], and (b) mean sea-level pressure [hPa] and 10 m winds [m s^{-1}] at 00 UTC on January 30, 2013 (NARR analysis data).

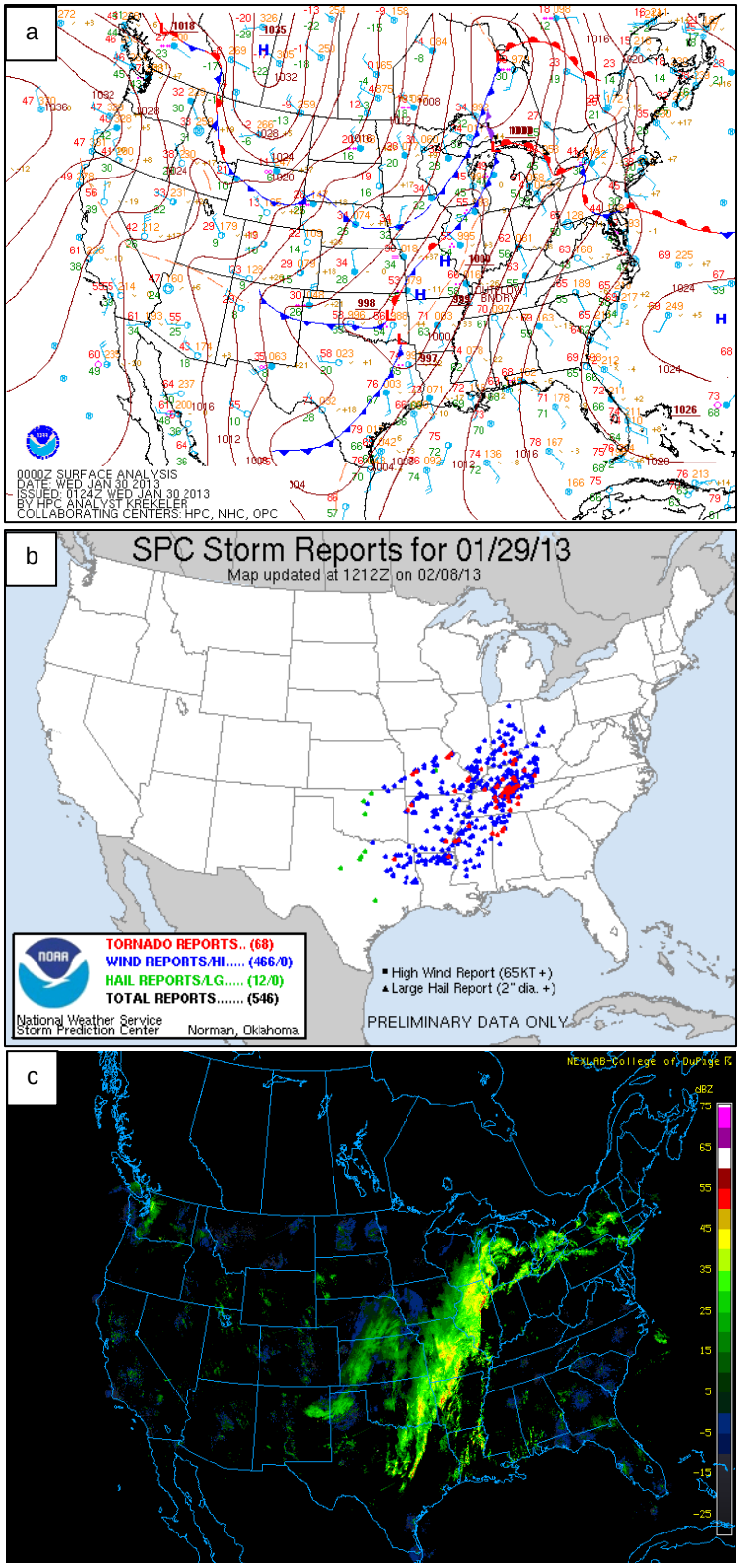

Fig. 3: (a) HPC Surface Analysis at 00 UTC on January 30, 2013, (b) SPC storm reports from 12 UTC January 29 to 12 UTC January 30, 2013, and (c) observed NEXRAD mosaic reflectivity from the College of DuPage site at approximately 00 UTC on January 30, 2013.

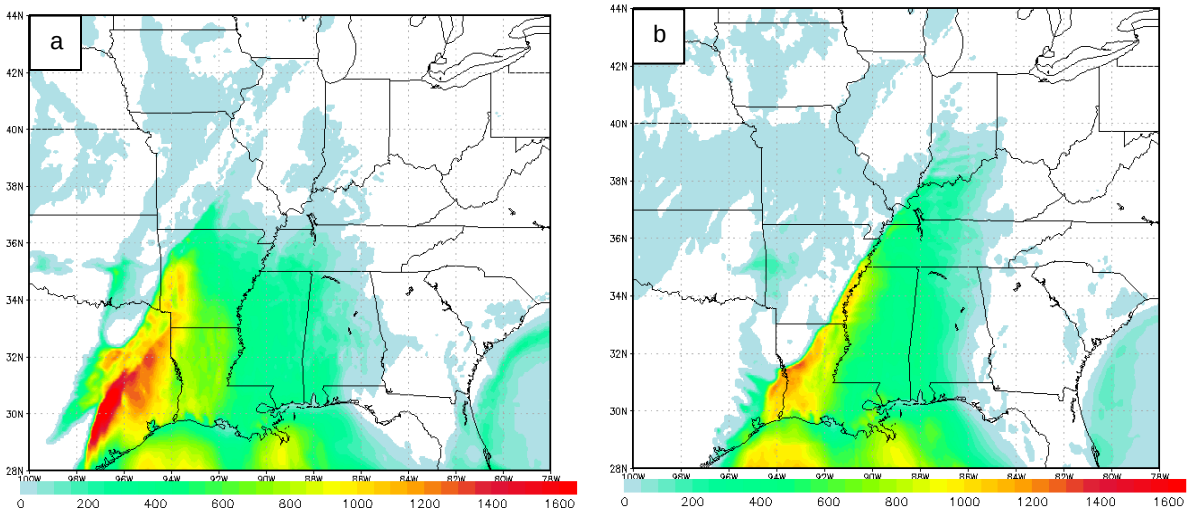

Fig. 4: WRF-simulated (domain 1) surface CAPE [J kg^{-1}] at (a) 00 UTC and (b) 06 UTC on January 30, 2013.

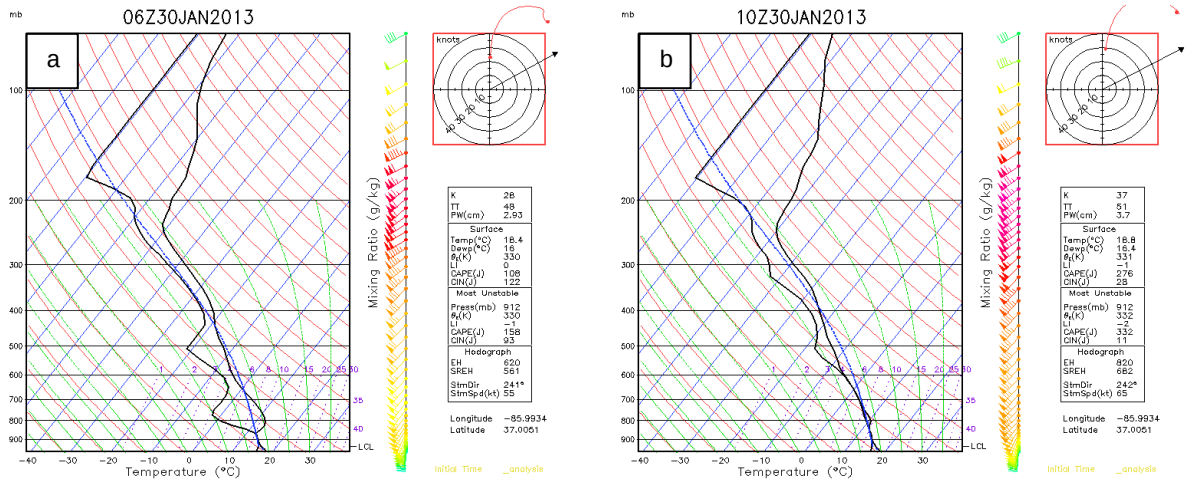

Fig. 5: WRF-simulated (domain 2) sounding from south-central Kentucky at (a) 06 UTC and (b) 10 UTC on January 30, 2013.

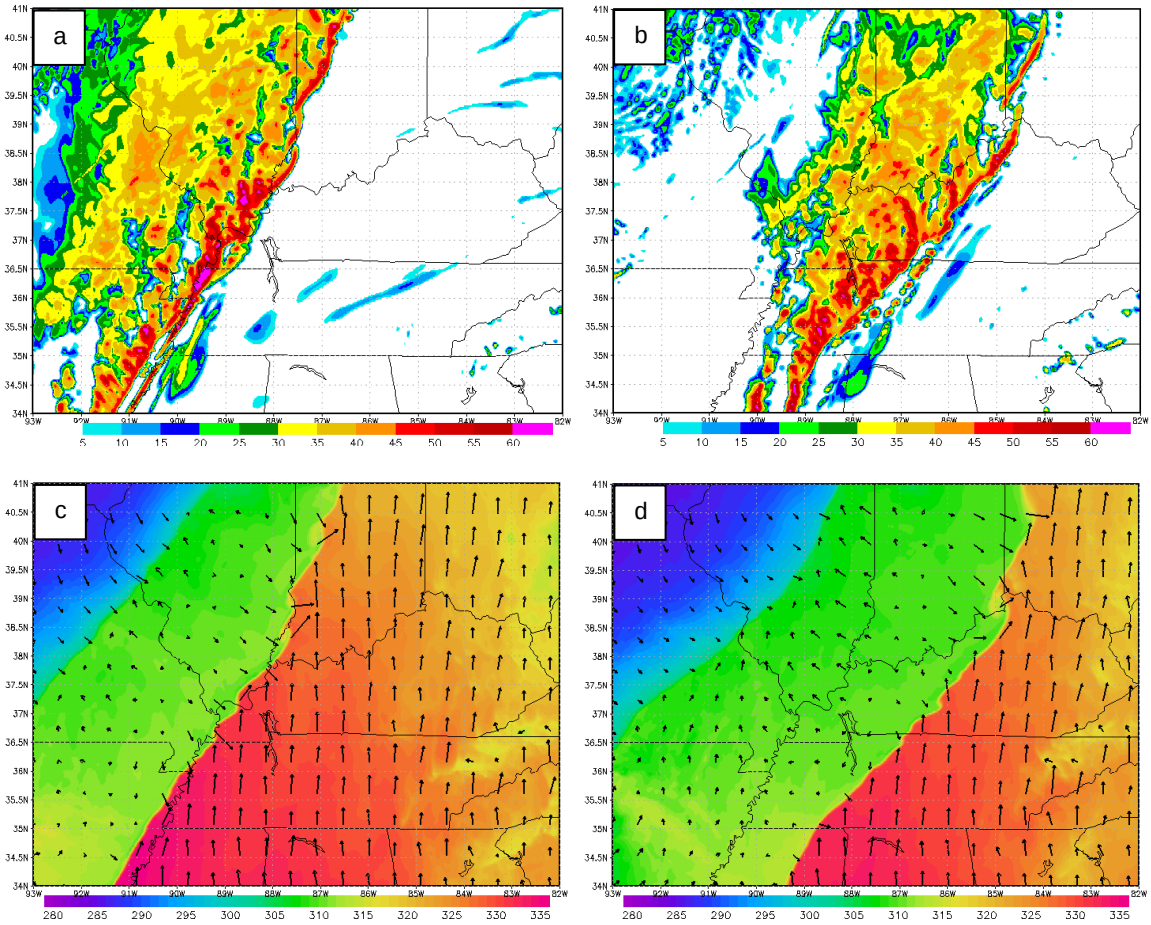

Fig. 6: WRF-simulated (domain 2) composite reflectivity [dBZ] from (a) 06 UTC and (b) 10 UTC, and surface equivalent potential temperature (θ_e) [K] from (c) 06 UTC and (b) 10 UTC on January 30, 2013.

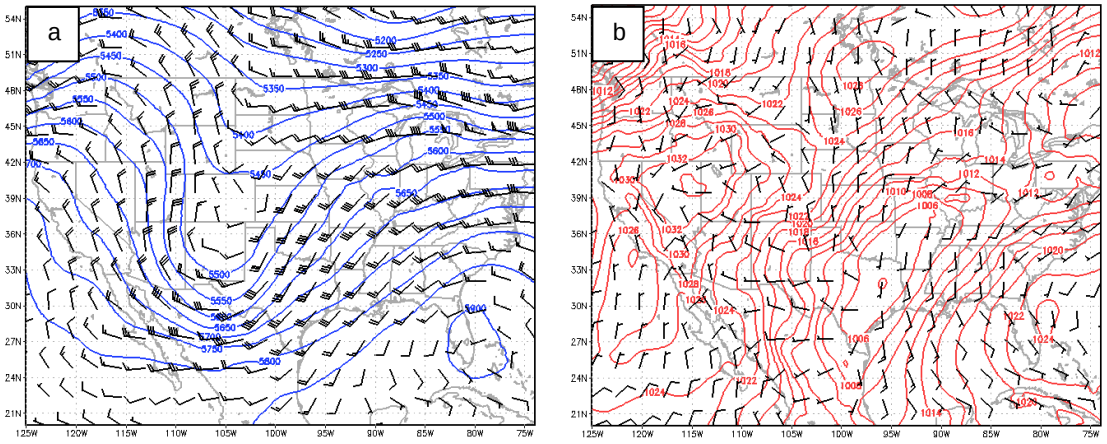

Fig. 7: Same as Fig. 2, except for 18 UTC on February 5, 2008.

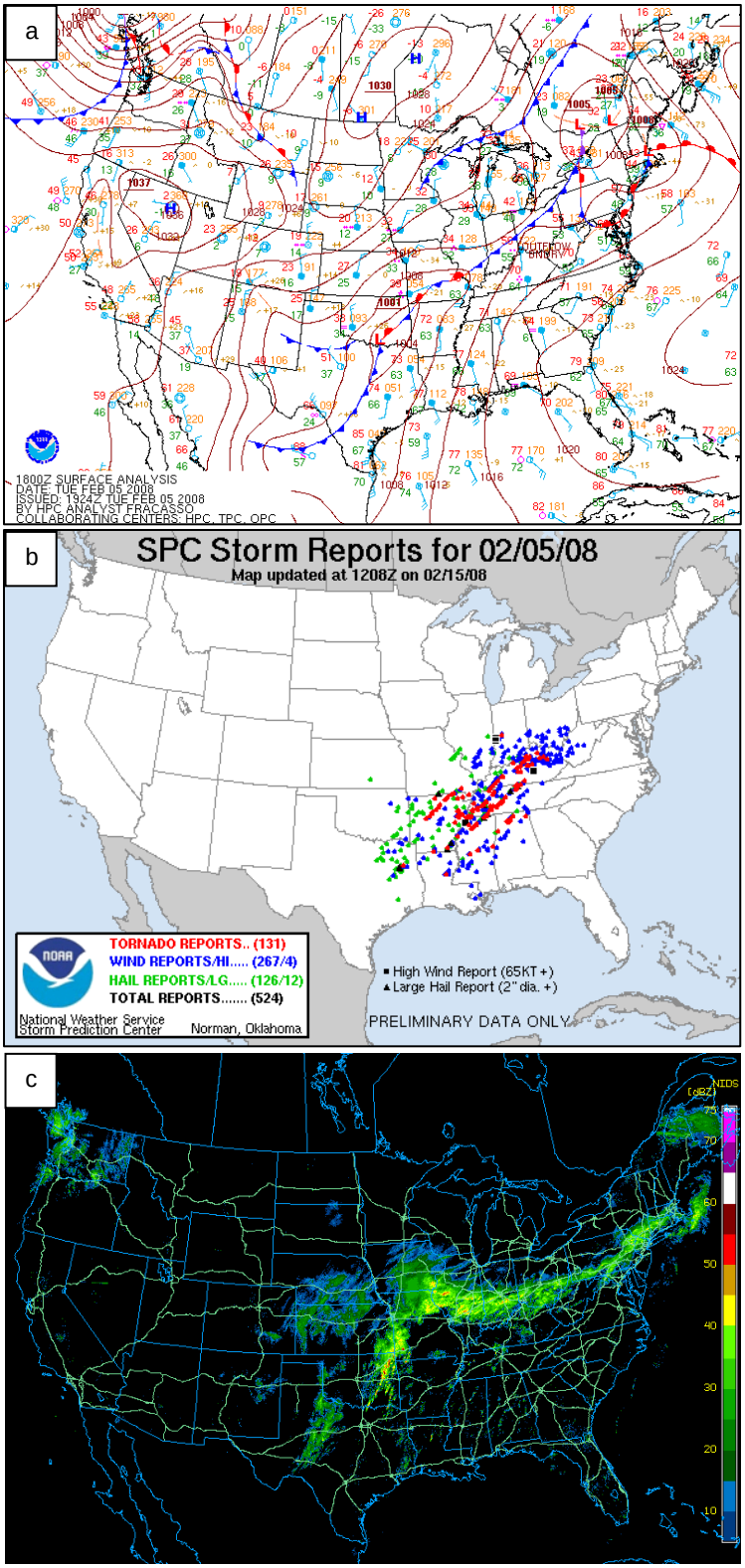

Fig. 8: (a) HPC Surface Analysis at 18 UTC on February 5, 2008, (b) SPC storm reports from 12 UTC February 5 to 12 UTC February 6, 2008, and (c) observed NEXRAD mosaic reflectivity from the College of DuPage site at approximately 18 UTC on February 5, 2008.

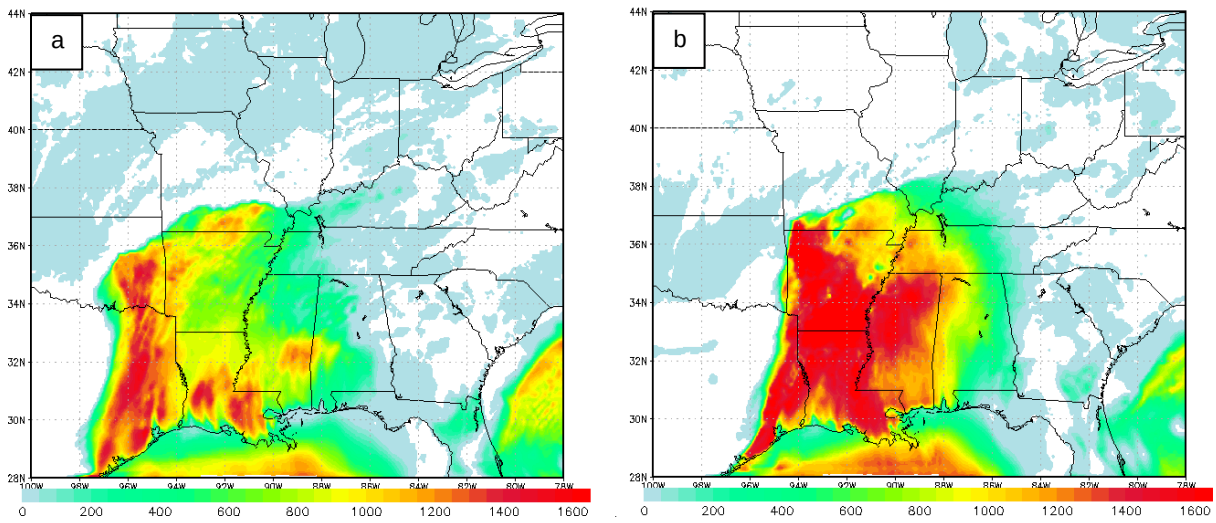

Fig. 9: Same as Fig. 4, except for (a) 17 UTC and (b) 23 UTC on February 5, 2008.

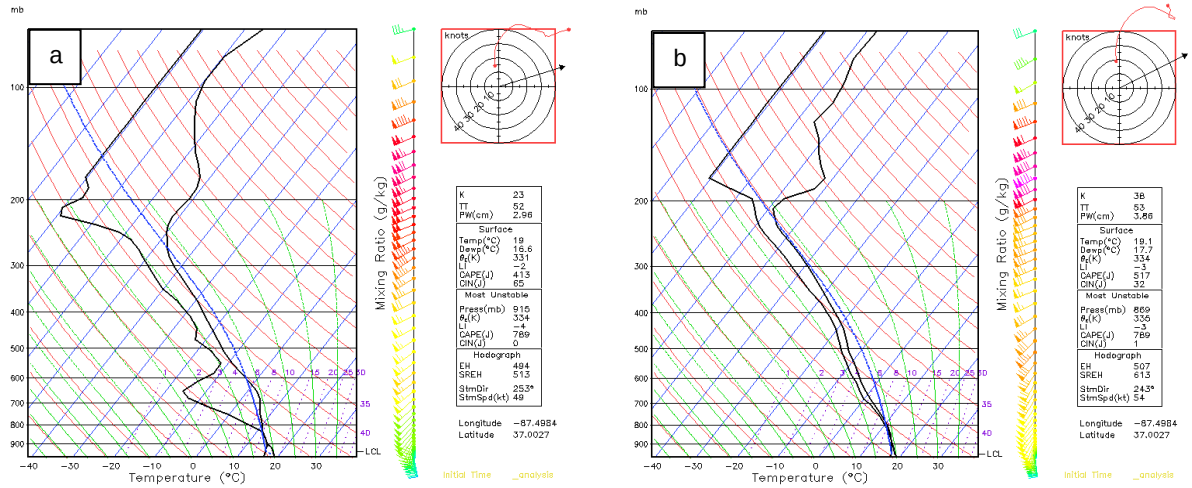

Fig. 10: Same as Fig. 5, except for (a) 23 UTC on February 5 and (b) 03 UTC on February 6, 2008 in southwestern Kentucky.

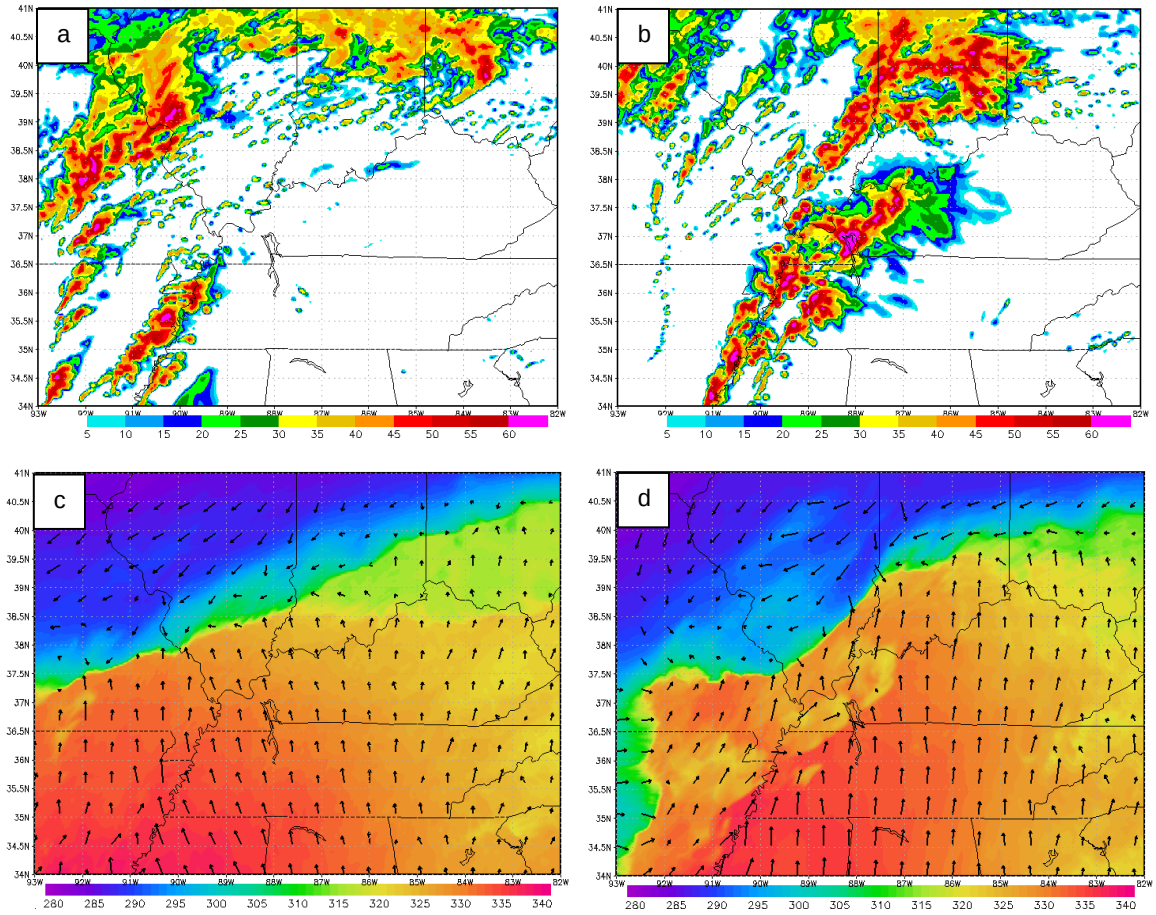

Fig. 11: Same as Fig. 6, except for (a), (c) 23 UTC on February 5 and (b), (d) 03 UTC on February 6, 2008.

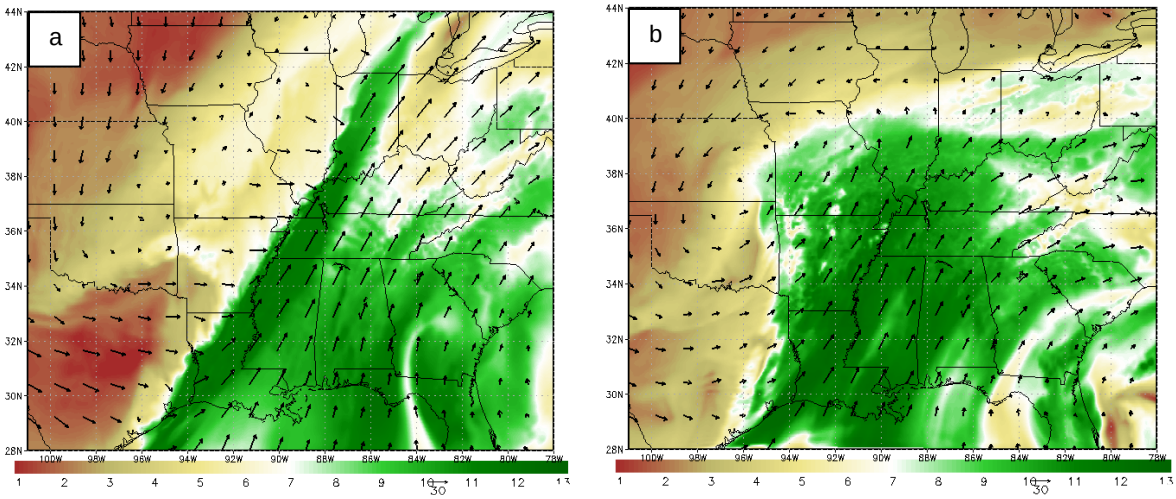

Fig. 12: WRF-simulated (domain 1) 850 hPa q_v [g kg^{-1}] and winds [m s^{-1}] for (a) 06 UTC on January 30, 2013, and (b) 23 UTC on February 5, 2008.

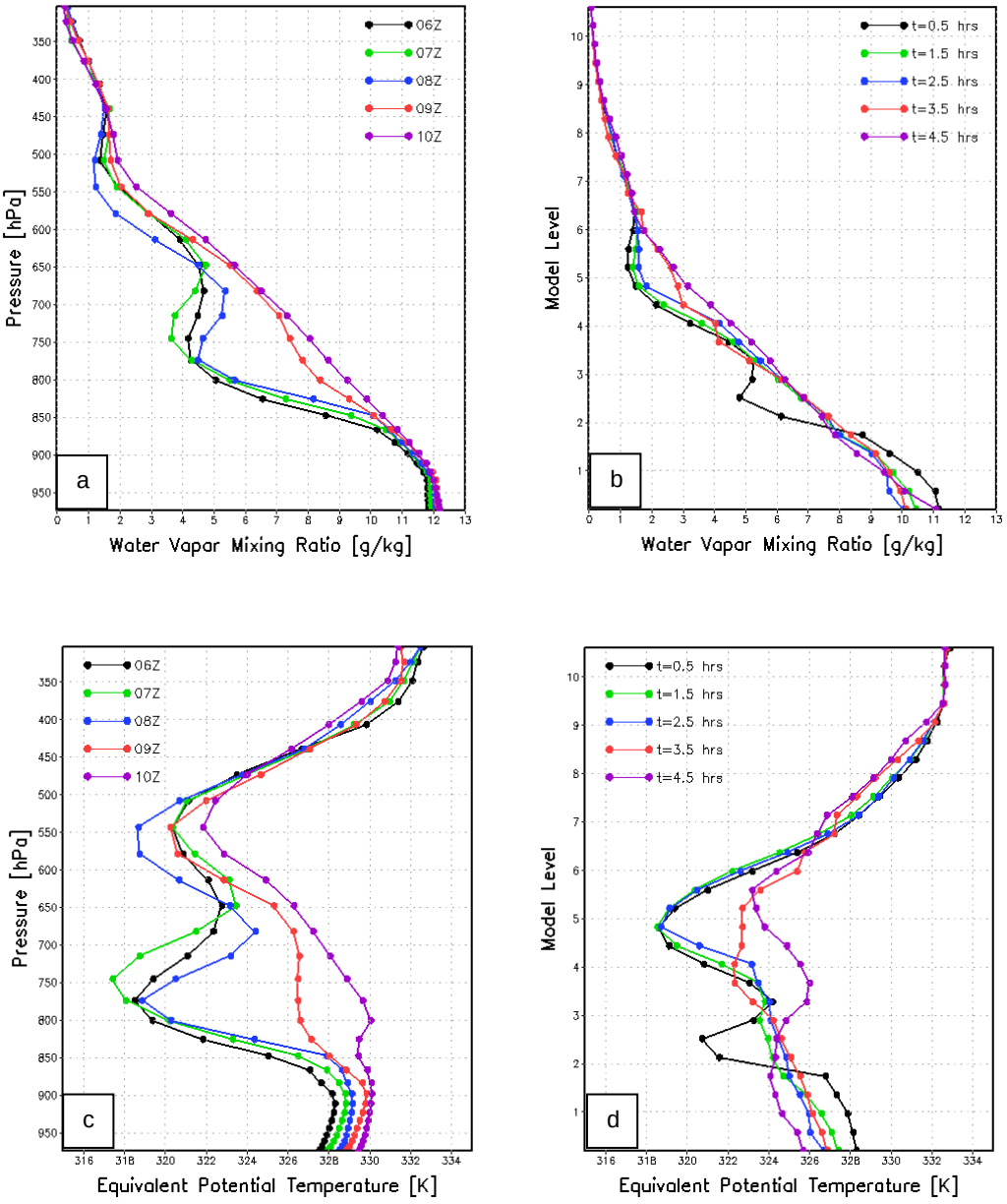

Fig. 13: Profiles from (a), (c) the WRF-simulated January 30, 2013 event in south-central Kentucky, and (b), (d) the CM1 idealized simulation. The profiles in (a) and (b) show θ_e, [K] and the profiles in (c) and (d) show q_v [g kg^{-1}] hourly for 5 hours in each simulation as the convective lines approaches.

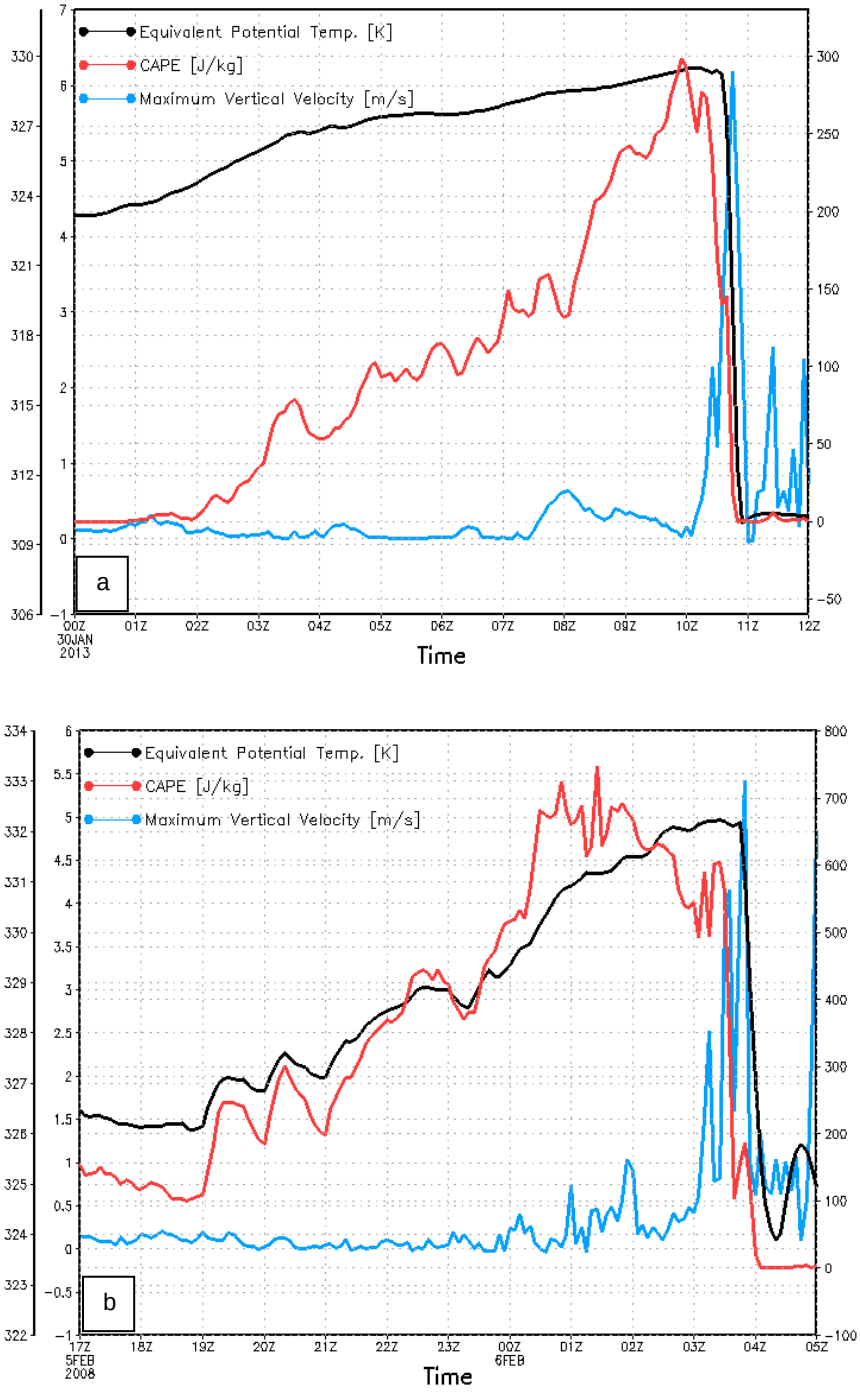

Fig. 14: WRF-simulated (domain 2) θ_e, CAPE, and maximum vertical velocity over time in for (a) the January 30, 2013 event, and (b) the February 5, 2008 event. The black, red and blue lines indicate θ_e, CAPE, and maximum vertical velocity, respectively. The leftmost vertical axis displays θ_e, [K] the right vertical axis displays CAPE [J kg^{-1}], and the inner left axis displays vertical velocity [m s^{-1}].